Mathematical appendix: CDC-42 encodes dynamically stable asymmetries in the *C. elegans* zygote via an incoherent feed-forward loop

Ondrej Maxian, Cassandra Azeredo-Tseng, Alex Anneken, Chris Schoff, Howard Clark, and Edwin Munro

April 30, 2024

1 Stability of myosin in maintenance phase

We first explore the dynamics of myosin alone, which we describe in terms of a one-dimensional spatially and temporally varying field $M(x,t)$ which evolves according to the advection-diffusion-reaction equations [1]

$$\partial_t M + \partial_x (vM) = D_M \partial_x^2 M + k_M^{\text{on}} M_{\text{cyto}} - k_M^{\text{off}} M \tag{M1a}$$

$$\gamma v = \eta \partial_x^2 v + \partial_x \sigma_a(M) \tag{M1b}$$

$$M_{\text{cyto}} = \frac{1}{hL}\left(M^{(\text{Tot})} L - \int_0^L M(x)\, dx \right), \tag{M1c}$$

where L is the domain length, h is the cytoplasmic thickness, and $M^{(\text{Tot})}$ is the density of myosin on the cortex when all of it is bound. The velocity field (M1b) comes from the assumption that myosin generates an active stress $\sigma_a(M)$, which combines with the viscous stress to give the total cortical stress $\sigma = \eta \partial_x v + \sigma_a(M)$. The force balance equation in the fluid says that the force due to stress must be balanced by the drag force, $\gamma v = \partial_x \sigma$, where γ is the drag coefficient. Combining the force balance with the stress expression gives the velocity equation (M1b), which can also be rewritten in terms of the "hydrodynamic lengthscale" $\ell = \sqrt{\eta/\gamma} \approx 14$ μm, which is essentially the lengthscale on which a local increase in the myosin field will pull in neighboring molecules [8]. As in [1], we ignore the elastic part of the stress, since the actomyosin cortex is purely viscous on timescales longer than the cortical turnover time [8].

To understand the threshold for instability of (M1), we scale the equations by appropriate time ($1/k_M^{\text{off}}$), length (L), density ($M^{(\text{Tot})}$), and velocity ($\sigma_0/\sqrt{\eta\gamma}$) scales. Defining the dimensionless (hatted) variables

$$x = \hat{x}L \qquad t = \hat{t}/k_M^{\text{off}} \qquad M = \hat{M}M^{(\text{Tot})} \qquad v = \hat{v}\frac{\sigma_0}{\sqrt{\eta\gamma}}, \tag{M2}$$

the resulting equations are

$$\partial_{\hat{t}}\hat{M} + \hat{\sigma}_0\partial_{\hat{x}}\left(\hat{v}\hat{M}\right) = \hat{D}_M\partial_{\hat{x}}^2\hat{M} + \hat{K}_M^{\text{on}}\left(1 - \int_0^1 \hat{M}(x)\,dx\right) - \hat{M} \tag{M3a}$$

$$\hat{v} = \hat{\ell}^2\partial_{\hat{x}}^2\hat{v} + \hat{\ell}\partial_{\hat{x}}\hat{\sigma}_a(\hat{M}) \tag{M3b}$$

and are controlled by the dimensionless parameters

$$\hat{\sigma}_0 = \left(\frac{\sigma_0/\sqrt{\eta\gamma}}{Lk_M^{\text{off}}}\right) \qquad \hat{D}_M = \frac{D_M}{k_M^{\text{off}}L^2} \qquad \hat{K}_M^{\text{on}} = \frac{k_M^{\text{on}}}{hk_M^{\text{off}}} \qquad \hat{\ell} = \frac{\sqrt{\eta/\gamma}}{L}. \tag{M4}$$

Recalling that $1/k_M^{\text{off}}$ is the residence time, these dimensionless parameters can be understood in the following way:

1. $\hat{\sigma}_0$ is the fraction of the domain over which a given myosin molecule is transported while it is bound to the membrane (the residence time $1/k_M^{\text{off}}$ $\times$ the advective velocity $\sigma_0/\sqrt{\eta\gamma}$).

2. $\hat{D}_M$ is the maximum fraction of the domain a molecule diffuses before it unbinds (in the extreme case when the gradient in the domain is $1/L$, the diffusive velocity is D_M/L).

3. $\hat{K}_M^{\text{on}}$ sets the uniform steady state of the model by $\hat{M}_0 = \hat{K}_M^{\text{on}}/\left(1 + \hat{K}_M^{\text{on}}\right)$.

4. $\hat{\ell}$ is the ratio of the hydrodynamic lengthscale (the lengthscale on which fluid flows can "grab" neighboring molecules) to the domain length.

Prior to performing linear stability analysis, we need to first determine the function σ_a and the other parameters.

1.1 Parameter estimation

Table 1 lists the parameters for the myosin model. According to [2], the *C. elegans* embryo has a roughly ellipsoidal shape, with half-axis lengths $27 \times 15 \times 15$ μm. The in-membrane diffusivity of myosin, as well as the detachment rate, have both been measured in [3]. For the attachment rate, it was estimated in [3, Fig. S3m] that roughly 30% of myosin is bound to the cortex in wild-type

Parameter	Description	Value	Units	Ref	Notes
L	Domain length	134.6	μm	[2]	radii 27×15 μm ellipse
D_M	Myosin diffusivity	0.05	$\mu\text{m}^2/\text{s}$	[3]	
$\hat{K}_M^{\text{on}}$	Myosin attachment rate	0.4			Fit to get 30% bound myosin
k_M^{off}	Myosin detachment rate	0.12	1/s	[3]	
η	Cytoskeletal fluid viscosity	0.1	Pa·s		$100 \times$ water
γ	Myosin drag coefficient	5×10^{-4}	$\text{Pa·s}/\mu\text{m}^2$		$\ell = \sqrt{\eta/\gamma} = 14\,\mu$m [8]
σ_0	Stress coefficient and form	0.0044	Pa		Fit in Sec. 1.1.1
$\hat{\sigma}_a(\hat{M})$	Stress function of myosin	$\hat{M}$			Fit in Sec. 1.1.1

Table 1: Parameter values for myosin model. Parameters listed with a citation are lifted directly from the corresponding study. See Section 1.1 for a discussion of the fitting procedure for the other parameters.

embryos. Recalling that the uniform steady state is $\hat{M}_0 = \hat{K}_M^{\text{on}} / \left(1 + \hat{K}_M^{\text{on}}\right)$, this gives $\hat{K}_M^{\text{on}} = 0.43$. The total amount of myosin scales out of the equations.

For the fluid parameters, we assume that the viscosity of the cytoskeletal fluid on the cortex is 100 times water, which gives 0.1 Pa·s. The "hydrodynamic length scale" of $\ell = \sqrt{\eta/\gamma} = 14$ μm, measured in [8, 11], then gives the myosin drag coefficient γ. But more important than either of these is the stress as a function of myosin concentration. We fit this from the wild-type data of [12] in the next section.

1.1.1 Inferring flow profile from experiments

Because we can measure the cortical velocity and myosin intensity, we can actually infer the function $\sigma_a(M)$ in dimensional units from the experimental data [12]. We in particular isolate the myosin intensity and flow speed during late maintenance phase in wild type embroys [12, Fig. 1B(bottom)], plotting the results in black in Fig. M1. For the myosin intensity, we simply use the raw values of fluorescence intensity without subtracting background, normalize so that the mean amount of bound myosin is 0.3 [3, Fig. S3], and adjust for the sensitivity of our measurements near the embryo edges by setting the myosin intensity at the outer 10% of the embryo to be constant and equal to that measured at the 10% boundary. We then periodically extend this data so that we fill the whole circumference (2 embryo lengths), and fit with a 3-term (4 terms including the constant) Fourier series.

To extract the stress profile from the smoothed velocity and myosin intensity, we consider a

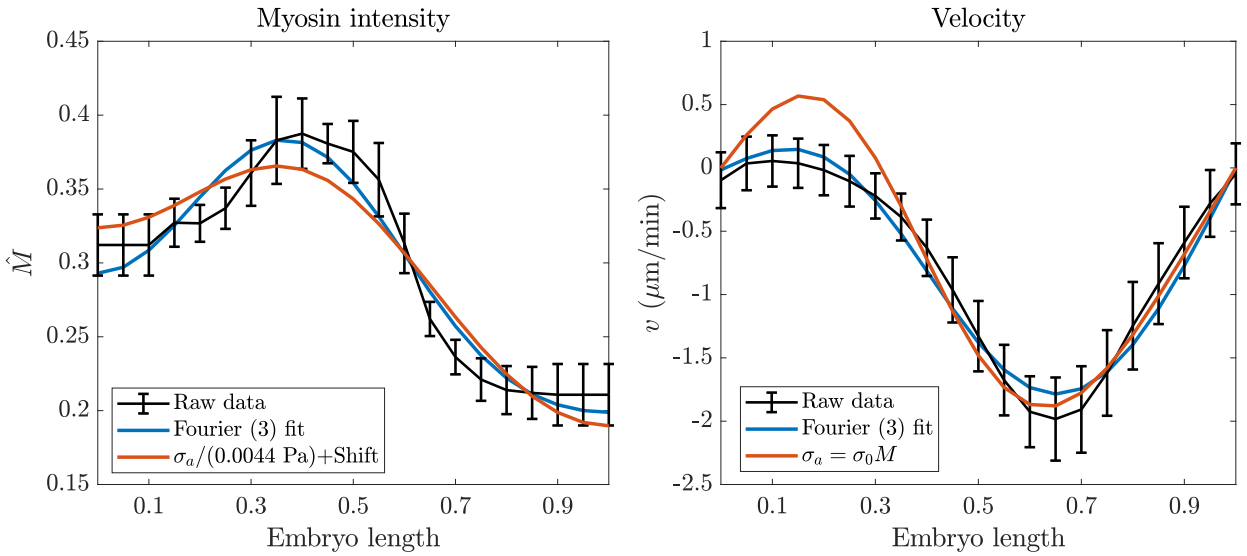

Figure M1: Extracting the active stress from the velocity profile. Left: the experimental data for myosin intensity (black with the outer 10% of the embryo on each side adjusted to be constant) and Fourier fit (blue), compared to the fitted stress (red). Right: velocity in μm/min (black) and Fourier fit (blue), compared to the velocity obtained when $\sigma_a = \sigma_0 M$.

hybrid dimensional form of the velocity equation (M1b),

$$\gamma v - \frac{\eta}{L^2}\partial_{\hat{x}}^2 v = \frac{1}{L}\partial_{\hat{x}}\sigma_a(M).$$

Let the Fourier series representation for $v(\hat{x}) = \sum_k \tilde{v}(k)\exp(2\pi i k\hat{x})$, and likewise for $\hat{\sigma}_a$. Then, in Fourier space, the solution for σ_a is given by

$$\sigma_a(k) = \frac{\gamma + \eta/L^2\,(2\pi k)^2}{2\pi i k/L}\tilde{v}(k). \tag{M5}$$

The $k = 0$ mode is undefined because σ_a only appears differentiated; thus stress is only available up to an arbitrary constant.

We insert the parameters from Table 1 into (M5), then rescale the resulting stress by $\sigma_0 = 4.4 \times 10^{-3}$ Pa plus an arbitrary constant, so that it aligns with the myosin intensity we determined experimentally. Using $\sigma_0 = 4.4 \times 10^{-3}$ Pa and the parameters in Table 1, the dimensionless parameter $\hat{\sigma}_0$ defined in (M4) is equal to

$$\hat{\sigma}_0 = \left(\frac{\sigma_0/\sqrt{\eta\gamma}}{L k_M^{\text{off}}}\right) \approx 0.04, \tag{M6}$$

which will control the stability analysis in the next section. The left panel of Fig. M1 also demonstrates that we can set

$$\hat{\sigma}_a = \hat{M} \tag{M7}$$

as a good approximation to the (dimensionless) stress. This plot is reproduced in Fig. 4A of the main text.

Notably, inserting the wild-type stress $\sigma_a = \sigma_0 M$ into the velocity equation gives the velocity profile shown in red in the right panel of Fig. M1. In the posterior, we obtain a velocity profile which perfectly matches the data, similar to the case when we fit stress in the left panel. In the anterior, on the other hand, there is a clear mismatch where the model predicts more contractility (flows into the myosin peak) than the data show. This demonstrates that there are additional agents inhibiting contractility in the anterior.

1.2 Linear stability analysis

Now that all the parameters are known, we can perform linear stability analysis to see if the system could spontaneously polarize. The uniform steady state is $\hat{M}_0 = \hat{K}_M^{\text{on}} / \left(1 + \hat{K}_M^{\text{on}}\right)$. We consider a perturbation around that state $\hat{M} = \hat{M}_0 + \delta\hat{M}$, where $\delta\hat{M} = \delta\hat{M}_0 e^{\lambda(k)\hat{t} + 2\pi i k\hat{x}}$. Plugging this into (M3b), we get the velocity [1, Eq. (11)]

$$\hat{v} = \frac{2\pi i k \hat{\ell} \hat{\sigma}_a'(\hat{M}_0)}{1 + \left(2\pi k \hat{\ell}\right)^2} \hat{\delta} M. \tag{M8}$$

Substituting this velocity into (M3a), and considering only the first order terms, we get the following equation for the eigenvalues

$$\lambda(k) = \frac{4\pi^2 k^2 \hat{\ell} \hat{M}_0 \hat{\sigma}_0 \hat{\sigma}_a'(\hat{M}_0)}{1 + 4\pi^2 k^2 \hat{\ell}^2} - \hat{D}_M 4\pi^2 k^2 - 1 \tag{M9}$$

Using the parameters in Table 1, we have the following values for the dimensionless groups

$$\hat{D}_M = 2.3 \times 10^{-5} \qquad \hat{M}_0 \approx 0.3 \qquad \hat{\sigma}_a' = 1 \qquad \hat{\ell} \approx 0.07. \tag{M10}$$

Substituting these parameters into the dispersion relation (M11) gives the eigenvalues $\lambda(k)$ shown in Fig. M2 as a function of wavelength k and dimensionless flow speed $\hat{\sigma}_0$. We observe strong flow coupling required for instability; with $\hat{\sigma}_0 = 0.2$ (flow transports myosins around 20% of the cell before they come off), the dynamics remain stable. Our estimate $\hat{\sigma}_0 \approx 0.04$ clearly demonstrates that myosin cannot self-polarize in the zygote.

Importantly, the large value of $\hat{\sigma}_0$ needed for instability is a consequence of the -1 in the dispersion relation (M11), which comes from the unbinding kinetics. Thus, unbinding makes it *harder* to destabilize the uniform steady state. Indeed, without the -1, the instability occurs at $\hat{\sigma}_0 \approx 10^{-3}$, which is pretty weak coupling to the flow (and weaker coupling than we observe

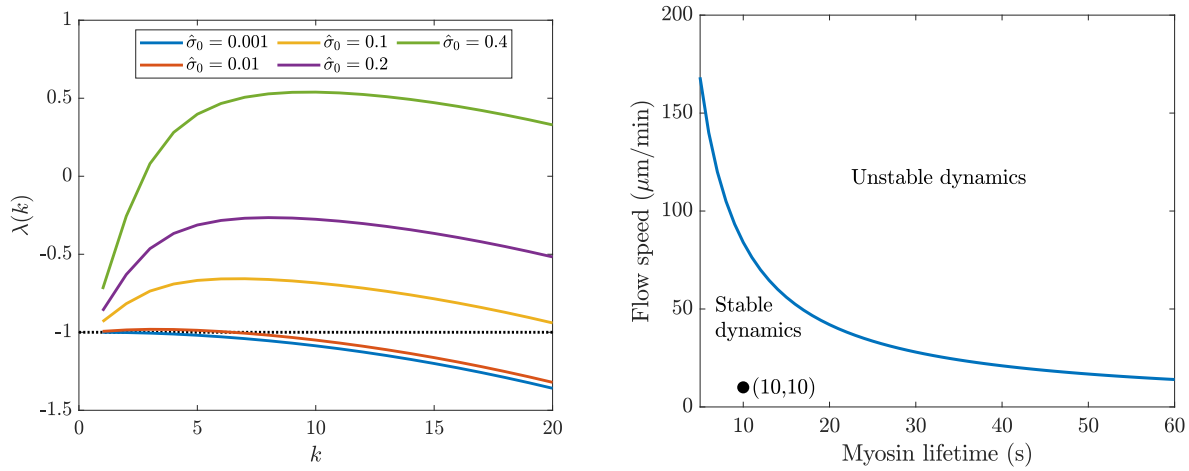

Figure M2: Stability analysis for myosin model (M3). Left: We consider perturbations of size proportional to $e^{\lambda(k)\hat{t}+2\pi ik\hat{x}}$, then solve the linearized form of (M3) to obtain $\lambda(k)$ in (M11). Positive eigenvalues indicate instability of the steady state. Eigenvalues above -1 indicate an unstable steady state in the absence of unbinding. Right: stability analysis for a simplified model without diffusion. We plot the required flow speeds $v = \ell/\tau_M$ for spontaneous polarization of myosin during maintenance phase, where $\tau_m = 1/k_M^{\text{off}}$ is the myosin lifetime and $\ell = 14$ μm is the hydrodynamic lengthscale. Flow speeds above the blue line give unstable dynamics, while flow speeds below it give stable dynamics.

experimentally). When we account for unbinding, diffusion becomes so small as to be irrelevant, as for the $k = 1$ mode the coefficient in (M11) is $\hat{D}_M 4\pi^2 \approx 10^{-3}$. Thus, the real balance here (to generate the instability) is not between advection and diffusion, but between advection and *unbinding*.

When we neglect diffusion in (M11), the largest eigenvalues occur when k is largest, so we can effectively take a limit as $k \to \infty$ to obtain

$$\lambda_\infty := \lambda(\hat{D}_M = 0; k \to \infty) = \frac{\hat{M}_0 \hat{\sigma}_0 \hat{\sigma}_a'}{\hat{\ell}^2} - 1 = \frac{\hat{M}_0 \left(\sigma_0/\sqrt{\eta\gamma}\right)}{\ell k_M^{\text{off}}} - 1 \tag{M11}$$

Recognizing $\sigma_0/\sqrt{\eta\gamma}$ as the velocity scale v, the condition $\lambda(k) > 0$ becomes equivalent to $v/k_M^{\text{off}} > \ell/\hat{M}_0$. Considering the most extreme case when $\hat{M}_0 = 1$ (all myosin bound to the membrane), we substitute $\ell \approx 14$ μm and plot the velocity threshold for instability as a function of myosin lifetime in the right panel of Fig. M2.

2 Maintenance phase biochemistry model

The equations which describe the biochemistry model are

$$\partial_t A_1 = D_A \partial_x^2 A_1 + \left(k_A^{\rm on} + k_A^+ f_A^+(A)\right) A_{\rm cyto} - k_A^{\rm off} A_1 \tag{M12a}$$
$$+ 2k_A^{\rm dp}(P)\hat{A}_2 - 2k_A^{\rm p}\hat{A_1}^2 + \sum_{n=3}^{N}\left(A_n - k_A^{\rm dp}(P)A_1 A_{n-1}\right)$$
$$\partial_t A_n = k_A^{\rm p} A_1 (A_{n-1} - A_n) - k_A^{\rm dp}(P)(A_n - A_{n+1}) \qquad N > n \geq 2 \tag{M12b}$$
$$\partial_t A_N = k_A^{\rm p} A_1 A_{N-1} - k_A^{\rm dp}(P) A_N \tag{M12c}$$
$$\partial_t C = D_C \partial_x^2 C + k_C^{\rm on} C_{\rm cyto} - k_C^{\rm off}\left(1 + r_{\rm PC} P\right) C \tag{M12d}$$
$$\partial_t K = D_K \partial_x^2 K + r_{\rm ACK} C \delta_{A>A_0} K_{\rm cyto} - k_K^{\rm off} K \tag{M12e}$$
$$\partial_t P = D_P \partial_x^2 P + k_P^{\rm on} P_{\rm cyto} - k_P^{\rm off}\left(1 + r_{\rm KP} K\right) P \tag{M12f}$$

The PAR-3 equations (M12a)–(M12c) describe the dynamics of PAR-3 oligomerization (an oligomer of size n denoted by A_n), for which we use the model developed in [5]. As discussed in detail there, the combination of oligomerization and positive feedback (through the term $k_A^+ f_A^+(A)$) imparts intrinsic bistability to the system. This bistability is strengthened when pPARs are included; through the term $k_A^{\rm dp}(P)$, these posterior PARs promote depolymerization of PAR-3.

PAR-3 also gates the association of CDC-42 with PAR-6/PKC-3 (K), which is a complex that inhibits all posterior PARs [6]. To model this, we work off the observations in [12], which reveal that PAR-6/PKC-3 are recruited to the membrane by CDC-42, provided that there is a sufficient concentration (roughly 10% of the enriched anterior level) of PAR-3 on the membrane. Thus the total loading term in (M13g) is proportional to the CDC-42 concentration times the cytoplasmic concentration of K, provided the PAR-3 concentration satisfies $A > A_0$. The other two equations (for CDC-42 and pPARs) are straightforward: we assume a basal rate of binding and unbinding, with an unbinding rate which is linearly enhanced by the inhibitor (pPARs for CDC-42 and PKC-3 for pPARs).

To fit missing parameters in (M12), we repeat the non-dimensionalization procedure we used for the myosin equation in Section 1 and in [5] for the PAR-3 equations. We scale lengths by L, time by $k_A^{\rm dp}$ (the typical time a molecule of PAR-3 spends on the membrane), and concentrations by the maximum when all protein is bound ($X^{(\rm Tot)}$ for protein X). The resulting dimensionless

equations are

$$\partial_{\hat{t}}\hat{A}_1 = \hat{D}_A\partial_{\hat{x}}^2 A_1 + \hat{K}_A^{\rm on}\left(1+\hat{K}_A^{\rm f}\hat{F}_A(\hat{A})\right)\left(1-\int_0^1 \hat{A}(x)\,d\hat{x}\right) - \hat{K}_A^{\rm off}\hat{A}_1 \tag{M13a}$$

$$+ 2\hat{A}_2 - 2\hat{K}_A^{\rm p}(\hat{P})\hat{A_1}^2 + \sum_{n=3}^{N}\left(\hat{A}_n - \hat{K}_A^{\rm p}(\hat{P})\hat{A}_1\hat{A}_{n-1}\right) \tag{M13b}$$

$$\partial_{\hat{t}}\hat{A}_n = \hat{K}_A^{\rm p}(\hat{P})\hat{A}_1(\hat{A}_{n-1}-\hat{A}_n) - (\hat{A}_n - \hat{A}_{n+1}) \qquad N > n \geq 2 \tag{M13c}$$

$$\partial_t\hat{A}_N = \hat{K}_A^{\rm p}(\hat{P})\hat{A}_1\hat{A}_{N-1} - \hat{A}_N, \tag{M13d}$$

for PAR-3, which are exactly those we used in [5], except that now the net polymerization rate $\hat{K}_{\rm AP}^{\rm p}$ is a function of P. To account for the inhibition of PAR-3 cluster growth by PAR-1 (P), we increase the effective depolymerization rate by setting

$$\hat{K}_{\rm AP}^{\rm p}(\hat{P}) = \frac{k_A^{\rm p}A^{(\rm Tot)}}{k_A^{\rm dp}\left(1+\hat{R}_{\rm PA}\hat{P}\right)} := \frac{\hat{K}_A^{\rm p}}{1+\hat{R}_{\rm PA}\hat{P}} \tag{M13e}$$

where $\hat{R}_{\rm PA} = r_{\rm PA}P^{(\rm Tot)}/k_A^{\rm dp}$ describes the rate at which pPARs inhibit cluster accumulation relative to the normal rate of depolymerization $k_A^{\rm dp}$. When $\hat{R}_{\rm PA} = 0$, we recover the dimensionless grouping $\hat{K}_A^{\rm p}$ used in [5]. Thus, all of the dimensionless parameters in the PAR-3 equations,

$$\hat{D}_A = \frac{D_A}{L^2k_A^{\rm dp}}, \quad \hat{K}_A^{\rm on} = \frac{k_A^{\rm on}}{k_A^{\rm dp}h}, \quad \hat{K}_A^{\rm f} = \frac{k_A^{+}A^{(\rm Tot)}}{k_A^{\rm on}}, \quad \hat{K}_A^{\rm off} = \frac{k^{\rm off}}{k_A^{\rm dp}} \qquad \hat{K}_A^{\rm p} = \frac{k_A^{\rm p}A^{(\rm Tot)}}{k_A^{\rm dp}},$$

with the exception of $\hat{R}_{\rm PA}$, are known from [5].

The dimensionless forms of the equations for CDC-42, PAR-6/PKC-3, and pPARs are

$$\partial_{\hat{t}}\hat{C} = \hat{D}_C\partial_{\hat{x}}^2\hat{C} + \hat{K}_C^{\rm on}\left(1-\int_0^1\hat{C}(\hat{x})\,d\hat{x}\right) - \hat{K}_C^{\rm off}\left(1+\hat{R}_{\rm PC}\hat{P}\right)\hat{C} \tag{M13f}$$

$$\partial_{\hat{t}}\hat{K} = \hat{D}_K\partial_{\hat{x}}^2\hat{K} + \hat{R}_{\rm ACK}\hat{C}\delta_{\hat{A}>\hat{A}_0}\left(1-\int_0^1\hat{K}(\hat{x})\,d\hat{x}\right) - \hat{K}_K^{\rm off}\hat{K} \tag{M13g}$$

$$\partial_{\hat{t}}\hat{P} = \hat{D}_P\partial_{\hat{x}}^2\hat{P} + \hat{K}_P^{\rm on}\left(1-\int_0^1\hat{P}(\hat{x})\,d\hat{x}\right) - \hat{K}_P^{\rm off}\left(1+\hat{R}_{\rm KP}\hat{K}\right)\hat{P}. \tag{M13h}$$

These equations reveal the following dimensionless groups

$$\hat{R}_{\rm PC} = \frac{r_{\rm PC}P^{(\rm Tot)}}{k_C^{\rm off}}, \quad \hat{R}_{\rm ACK} = \frac{r_{\rm ACK}C^{(\rm Tot)}}{k_A^{\rm dp}h}, \quad \hat{R}_{\rm KP} = \frac{r_{\rm KP}K^{(\rm Tot)}}{k_P^{\rm off}} \tag{M14a}$$

$$\hat{K}_P^{\rm on} = \frac{k_P^{\rm on}}{k_A^{\rm dp}h}, \quad \hat{K}_C^{\rm on} = \frac{k_C^{\rm on}}{k_A^{\rm dp}h}, \quad \hat{A}_0 = \frac{A_0}{A^{(\rm Tot)}} \tag{M14b}$$

$$\hat{D}_P = \frac{D_P}{L^2k_A^{\rm dp}}, \quad \hat{D}_C = \frac{D_C}{L^2k_A^{\rm dp}}, \quad \hat{D}_K = \frac{D_K}{L^2k_A^{\rm dp}}, \quad \hat{K}_P^{\rm off} = \frac{k_P^{\rm off}}{k_A^{\rm dp}}, \quad \hat{K}_K^{\rm off} = \frac{k_K^{\rm off}}{k_A^{\rm dp}}, \quad \hat{K}_C^{\rm off} = \frac{k_C^{\rm off}}{k_A^{\rm dp}} \tag{M14c}$$

Parameter	Description	Value	Units	Ref	Notes
D_P	pPAR diffusivity	0.15	$\mu\text{m}^2/\text{s}$	[2]	
D_K	PAR-6 diffusivity	0.1	$\mu\text{m}^2/\text{s}$	[10]	
D_C	CDC-42 diffusivity	0.1	$\mu\text{m}^2/\text{s}$		Same as PAR-6
k_P^{off}	pPAR detachment rate	7.3×10^{-3}	1/s	[2]	
k_K^{off}	PAR-6 detachment rate	0.01	1/s	[10]	
k_C^{off}	CDC-42 detachment rate	0.01	1/s		Same as PAR-6
$\hat{K}_P^{\text{on}}$	PAR-2 attachment rate	0.09			$P \approx 1$ in enrichment zone
$\hat{R}_{\text{KP}}$	K inhibiting P	50			Strong inhibition
$\hat{R}_{\text{PC}}$	P inhibiting C	(M16)		[12]	CDC/CHIN-1 relationship (Fig. A5)
$\hat{K}_C^{\text{on}}$	CDC-42 attachment rate	0.07			20% bound with inhibition
$\hat{A}_0$	PAR-3 threshold for PAR-6	0.06		[12]	10% anterior level
$\hat{R}_{\text{ACK}}$	A and C creating K	0.1			20% bound K
$\hat{R}_{\text{PA}}$	P inhibiting A	2			80% monomers on posterior in wild-type

Table 2: Additional parameter values for the biochemistry model.

Among these, the parameters in (M14c) are all known from literature, and have been reported in the top half of Table 2. This leaves the six parameters in (M14a) and (M14b), which we determine sequentially from the following set of experimental observations:

1. In embryos without myosin flows, roughly 25–30% of the available PAR-2 is bound at steady state [3, Fig. S3]. Because the PAR-2 domain is only 25–30% of the embryo, the concentration of P in its enrichment zone must be near 1. We find that $\hat{K}_P^{\text{on}} = 0.09$ reproduces this result (in dimensional units $k_P^{\text{on}} = 0.13$ μm/s [3]).

2. In embryos without myosin flows, the level of PAR-2 at the anterior is no more than 5% of the posterior level [3, Fig. 2c]. This sets $\hat{R}_{\text{KP}} \gg 1$. We use $\hat{R}_{\text{KP}} = 50$ for strong inhibition.

3. The parameter $\hat{R}_{\text{PC}}$ is available from the data in [12]. To obtain it, we solve (M13f) at steady state to obtain

$$\hat{C} = \frac{1}{1 + \frac{hk_c^{\text{off}}}{k_C^{\text{on}}} + \frac{\hat{R}_{\text{PC}} k_C^{\text{off}} h}{k_C^{\text{on}}} \hat{P}}. \tag{M15}$$

   If we normalize so that $\hat{C} = 1$ when $\hat{P} = 0$, we obtain

$$\tilde{C} := \frac{1 + \frac{hk_c^{\text{off}}}{k_C^{\text{on}}}}{1 + \frac{hk_c^{\text{off}}}{k_C^{\text{on}}} + \frac{\hat{R}_{\text{PC}} k_C^{\text{off}} h}{k_C^{\text{on}}} \hat{P}}$$

Now according to [12], $\tilde{C} \approx 1/(1+13.3\hat{P})$, which implies that

$$13.3 = \frac{\hat{R}_{\mathrm{PC}} k_C^{\mathrm{off}} h}{k_C^{\mathrm{on}} \left(1 + \frac{h k_c^{\mathrm{off}}}{k_C^{\mathrm{on}}}\right)} = \frac{\hat{R}_{\mathrm{PC}} k_C^{\mathrm{off}} h}{k_C^{\mathrm{on}} + h k_c^{\mathrm{off}}} \rightarrow \hat{R}_{\mathrm{PC}} = 13.3 \left(1 + \frac{k_C^{\mathrm{on}}}{k_C^{\mathrm{off}} h}\right). \tag{M16}$$

This relationship defines $\hat{R}_{\mathrm{PC}}$ for given k_C^{on} and k_C^{off}.

4. In [3, Fig. S3i], it is reported that roughly 25% of PAR-6 is bound in wild-type embryos. Assuming that CDC-42 has a similar set of properties, we can assume 25% of the protein is bound. Setting $\hat{K}_C^{\mathrm{on}} = 0.07$ and combining with the inhibition strength (M16) gives about 20% bound CDC-42 at steady state (in dimensional units $k_C^{\mathrm{on}} = 0.1$ μm/s).

5. If 25% of CDC-42 is bound, we have $\hat{C} = 0.25$, and our goal is to set $\hat{R}_{\mathrm{ACK}}$ to obtain about 25% bound PAR-6 (when there is sufficient PAR-3) as well. Plugging this into the steady state version of (M13g), we obtain

$$\hat{R}_{\mathrm{ACK}}(0.25)(0.75) - (0.0625)(0.25) = 0 \rightarrow \hat{R}_{\mathrm{ACK}} = 0.08 \approx 0.1.$$

6. In embryos depleted of PAR-1 and CHIN-1, the level of PAR-3 at the anterior is roughly 10% of the posterior, and PAR-6 can load onto the membrane everywhere. We therefore set $\hat{A}_0 = 0.06$, since we've already tuned the PAR-3 parameters so that the polarized state has $\hat{A} \approx 0.6$ on the anterior and $\hat{A} \approx 0.06$ on the posterior [5].

This fitting procedure, which is summarized Table 2, gives values for all parameters except $\hat{R}_{\mathrm{PA}}$. This parameter is more important than the rest, as we show in the next section, because it sets the steady state bistable behavior.

2.1 How inhibition of PAR-3 oligomerization dictates behavior

As discussed in [5], the PAR-3 dynamics in (M13) are intrinsically bistable; they set up a stable A/P boundary even in the absence of the posterior inhibitor PAR-1. Nevertheless, inhibition by PAR-1 can affect the steady state boundary position, as well as the dynamics of the other proteins. To understand this further, we set up an initial condition shown in the top left of Fig. M3, where PAR-3 (A) is enriched in the middle 50% of the embryo, while posterior PARs (P) are enriched in the outer 50%. CDC-42 (C) is distributed uniformly, and no PAR-6/PKC-3 (K) is bound to the membrane. We then run the model forward in time until $\hat{t} = 200$ (20 minutes of real time) and look at how the distributions of the proteins evolve.

Based on the results in Fig. M3, we distinguish three different regimes of inhibition:

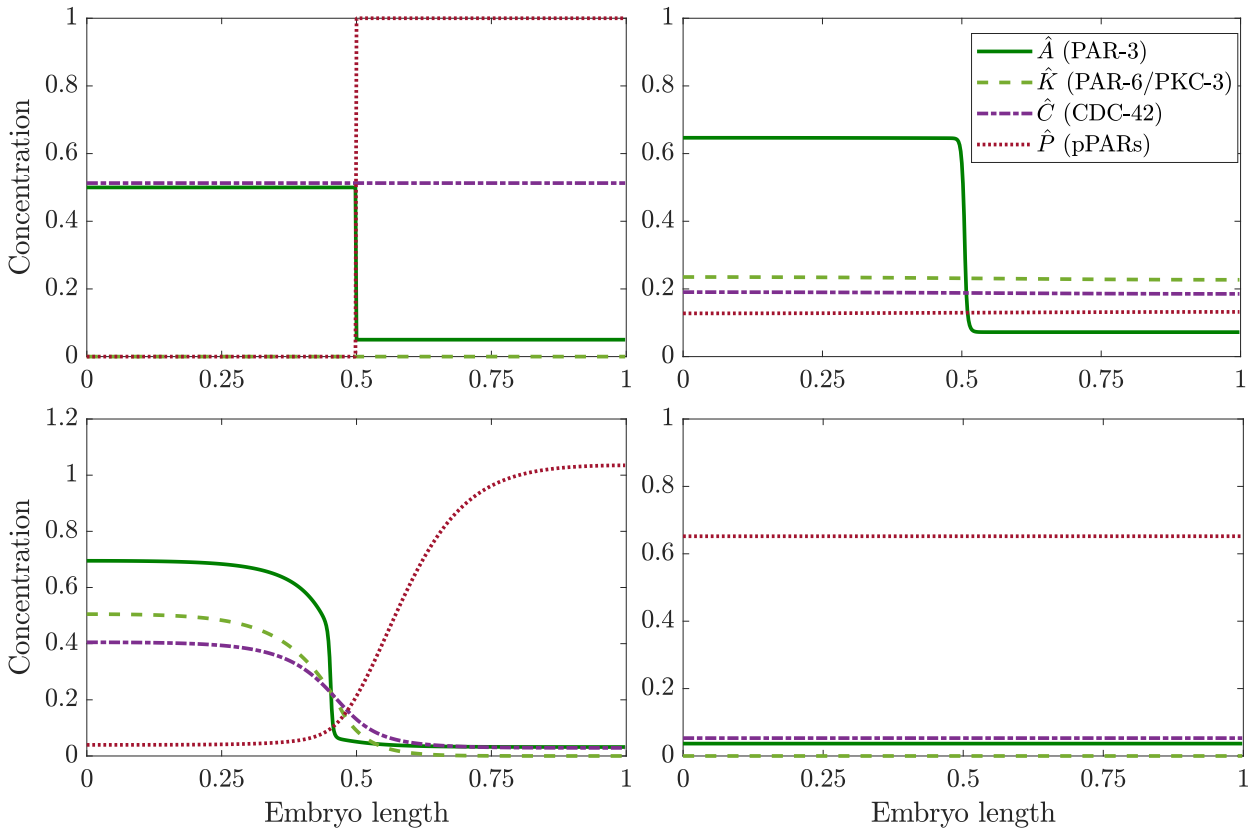

Figure M3: Dynamics of biochemistry model (M12) with different strengths of PAR-3 cluster inhibition by PAR-1 (parameter $\hat{R}_{\mathrm{PA}}$). Top left: the initial condition we use for the simulations. PAR-3 (A) is enriched in the middle 50% of the embryo, while posterior PARs (P) are enriched in the outer 10%. CDC-42 (C) is distributed uniformly, and no PAR-6/PKC-3 (K) is bound to the membrane. The next three plots show the state at $\hat{t} = 200$ (about 20 minutes of real time) with three different values of $\hat{R}_{\mathrm{PA}}$.

1. In the regime where $\hat{R}_{\mathrm{PA}}$ is small (top right), there is not enough inhibition of PAR-3 to prevent it from accumulating on the posterior at 10% of its anterior level. Because of this, the PAR-6/PKC-3 complex accumulates uniformly on the membrane. Consequently, posterior PARs and CDC-42 all accumulate uniformly (there are still some small residual asymmetries left over from the initial data in the plot).

2. In the regime where $\hat{R}_{\mathrm{PA}}$ is large (bottom right), a small amount of pPARs are sufficient to reduce oligomerization of PAR-3 and destroy the bistability. In this case, pPARs outcompete PAR-3, which sets up a state where *all* of the proteins are distributed uniformly (PAR-6/PKC-3 cannot load onto the membrane anywhere because the PAR-3 concentration is too low).

3. For intermediate values of $\hat{R}_{\mathrm{PA}}$ (bottom left, the exact range is $1 \lesssim \hat{R}_{\mathrm{PA}} \lesssim 20$), PAR-1 locally drives PAR-3 into its monomer form, which leads to more unbinding. In these regions, the pPARs outcompete PAR-3 and bind to the membrane, and there is a steady state where PAR-3 and the pPARs are separated by a buffer zone of PAR-6/PKC-3.

Obviously, the wild-type system must fall into the third regime.

2.1.1 Setting the inhibition strength $\hat{R}_{\mathrm{PA}}$ based on steady states

When we operate in the regime where there is stable polarized state (PAR-3 enriched in half the embryo, pPARs enriched in the other half), the parameter $\hat{R}_{\mathrm{PA}}$ also affects the distribution of oligomer sizes on the posterior. At steady state, this is an exponential distribution, with $\alpha(\hat{x}) = \hat{K}_{\mathrm{AP}}\left(\hat{P}(\hat{x})\right)\hat{A}_1(\hat{x})$ expressing the exponent [7, 5], and $(1-\alpha)^2$ the fraction of protein in monomer form. To determine the value of $\hat{R}_{\mathrm{PA}}$, we simulate to steady state with several different values, and plot the PAR-3 domain size over time and α values. To mimic the onset maintenance phase, we start the system in a state where 50% of the domain is enriched in PAR-3, then watch the boundary expand/contract.

When we start the system at the end of establishment phase, we find that the PAR-3 boundary is quasi-stable when $\hat{R}_{\mathrm{PA}} \leq 2$. For $\hat{R} > 2$, there is a shift to a smaller domain size on a timescale of $\hat{t} = 100$ (10 minutes of real time). Because the system is in a quasi-stable state, it is logical to look at the α value on the posterior as a way to constrain the value of $\hat{R}_{\mathrm{PA}}$. Figure M4 shows that $\alpha = 0.42$ without PAR-1 inhibition (30% in monomer form) [5], while when $\hat{R}_{\mathrm{PA}} = 1, 2$, and 4 we have $\alpha = 0.19$, 0.12, and 0.08, respectively. These values of α correspond roughly to 65, 75, and

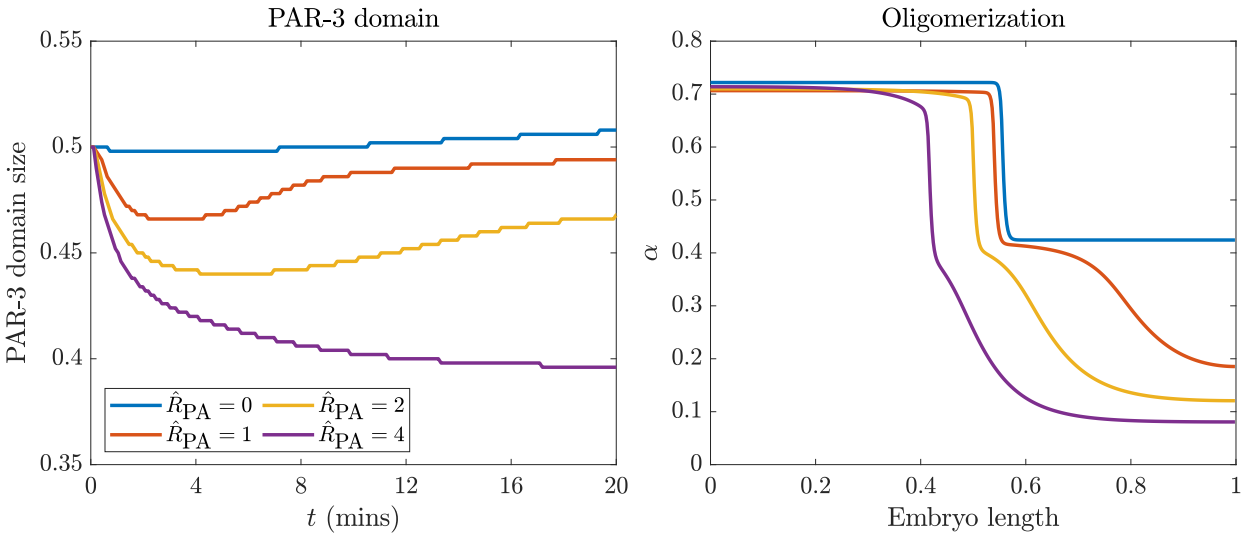

Figure M4: Steady state domain sizes and oligomerization kinetics with biochemistry model (M12), varying parameter $\hat{R}_{\mathrm{PA}}$. We show the PAR-3 domain size over time (left) and α values at steady state (right) for three different values of $\hat{R}_{\mathrm{PA}}$.

85% in monomer form. We choose $\hat{R}_{\mathrm{PA}} = 2$, so that the steady state has roughly 75% in monomer form on the posterior. With this value, the steady state A/P ratio of PAR-3 goes from about 7:1 without P inhibition to 20:1 with P inhibition, which qualitatively matches the experimental dynamics of a roughly 5 fold change [12, Fig. 4c].

3 Coupling contractility to biochemistry

We obtain the dimensionless equations which couple biochemistry and contractility via a straightforward combination of (M3) and (M12), advecting all proteins with the myosin flow field [4], and making CDC-42 a promoter of myosin. The resulting equations are

$$\partial_{\hat{t}}\hat{A}_1 + \hat{\sigma}_0\partial_{\hat{x}}\left(\hat{v}\hat{A}_1\right) = \hat{D}_A\partial_{\hat{x}}^2 A_1 + \hat{K}_A^{\rm on}\left(1+\hat{K}_A^{\rm f}\hat{F}_A(\hat{A})\right)\left(1-\int_0^1 \hat{A}(x)\,d\hat{x}\right) - \hat{K}_A^{\rm off}\hat{A}_1 \tag{M17a}$$
$$+ 2\hat{A}_2 - 2\hat{K}_{\rm AP}^{\rm p}{\hat{A}_1}^2 + \sum_{n=3}^{N}\left(\hat{A}_n - \hat{K}_{\rm AP}^{\rm p}\hat{A}_1\hat{A}_{n-1}\right)$$
$$\partial_{\hat{t}}\hat{A}_n + \hat{\sigma}_0\partial_{\hat{x}}\left(\hat{v}\hat{A}_n\right) = \hat{K}_{\rm AP}^{\rm p}\hat{A}_1(\hat{A}_{n-1}-\hat{A}_n) - (\hat{A}_n - \hat{A}_{n+1}) \qquad N > n \geq 2 \tag{M17b}$$
$$\partial_{\hat{t}}\hat{A}_N + \hat{\sigma}_0\partial_{\hat{x}}\left(\hat{v}\hat{A}_N\right) = \hat{K}_{\rm AP}^{\rm p}\hat{A}_1\hat{A}_{N-1} - \hat{A}_N \tag{M17c}$$
$$\partial_{\hat{t}}\hat{C} + \hat{\sigma}_0\partial_{\hat{x}}\left(\hat{v}\hat{C}\right) = \hat{D}_C\partial_{\hat{x}}^2\hat{C} + \hat{K}_C^{\rm on}\left(1-\int_0^1 \hat{C}(\hat{x})\,d\hat{x}\right) - \hat{K}_C^{\rm off}\left(1+\hat{R}_{\rm PC}\hat{P}\right)\hat{C} \tag{M17d}$$
$$\partial_{\hat{t}}\hat{K} + \hat{\sigma}_0\partial_{\hat{x}}\left(\hat{v}\hat{K}\right) = \hat{D}_K\partial_{\hat{x}}^2\hat{K} + \hat{R}_{\rm ACK}\hat{C}\delta_{\hat{A}>\hat{A}_0}\left(1-\int_0^1 \hat{K}(\hat{x})\,d\hat{x}\right) - \hat{K}_K^{\rm off}\hat{K} \tag{M17e}$$
$$\partial_{\hat{t}}\hat{P} + \hat{\sigma}_0\partial_{\hat{x}}\left(\hat{v}\hat{P}\right) = \hat{D}_P\partial_{\hat{x}}^2\hat{P} + \hat{K}_P^{\rm on}\left(1-\int_0^1 \hat{P}(\hat{x})\,d\hat{x}\right) - \hat{K}_P^{\rm off}\left(1+\hat{R}_{\rm KP}\hat{K}\right)\hat{P} \tag{M17f}$$
$$\partial_{\hat{t}}\hat{M} + \hat{\sigma}_0\partial_{\hat{x}}\left(\hat{v}\hat{M}\right) = \hat{D}_M\partial_{\hat{x}}^2\hat{M} + \hat{K}_M^{\rm on}\left(1+\hat{R}_{\rm CM}\hat{C}\right)\left(1-\int_0^1 \hat{M}(x)\,dx\right) - \hat{K}_M^{\rm off}\hat{M} \tag{M17g}$$
$$\hat{v} = \hat{\ell}^2\partial_{\hat{x}}^2 v + \hat{\ell}\partial_{\hat{x}}\hat{\sigma}_a(\hat{M}) \tag{M17h}$$
$$\hat{R}_{\rm CM} = \frac{r_{\rm CM}C^{(\rm Tot)}}{k_M^{\rm on}},\ \hat{D}_M = \frac{D_M}{L^2k_A^{\rm dp}},\ \hat{K}_M^{\rm on} = \frac{k_M^{\rm on}}{hk_A^{\rm dp}},\ \hat{K}_M^{\rm off} = \frac{k_M^{\rm off}}{k_A^{\rm dp}},\ \hat{\sigma}_0 = \frac{\sigma_0/\sqrt{\eta\gamma}}{Lk_A^{\rm dp}},\ \hat{\ell} = \frac{\sqrt{\eta/\gamma}}{L}. \tag{M17i}$$

The last equation (M17i) defines the key *new* dimensionless parameters relating to myosin. These differ from (M4) because we can only non-dimensionalize time by one quantity, and we choose here to stick with the depolymerization time $1/k_A^{\rm dp}$. Table 1 gives the dimensional quantities D_M, σ_0 and $k_M^{\rm off}$, from which we obtain $\hat{D}_M$, $\hat{\sigma}_0$ and $\hat{K}_M^{\rm off}$. This leaves two parameters which control the myosin profile: the basal rate $k_M^{\rm on}$, and the amount that CDC-42 promotes myosin, $\hat{R}_{\rm CM}$. In wild-type embryos, we estimate the minimum amount of bound myosin (in the absence of CDC-42) as 0.2. This sets $k_M^{\rm on}$ via $k_M^{\rm on}/(k_M^{\rm on}+k_M^{\rm off}h) \approx 0.2$, giving $k_M^{\rm on} = 0.3$ μm/s.

The parameter $\hat{R}_{\rm CM} = 8$ is then chosen to match the initial speed of maintenance phase rescue (flow speed 2 μm/min). The simulations in main text Fig. 3 (without branched actin) use $\hat{R}_{\rm CM} = 5$ while the ones in Fig. 6 use $\hat{R}_{\rm CM} = 8$.

Parameter	Description	Value	Units	Ref	Notes
D_R	Branched actin diffusivity	0.1	$\mu\text{m}^2/\text{s}$		Same as CDC-42
k_R^{off}	Branched actin unbinding rate	0.12	$1/\text{s}$		Same as myosin
$\hat{R}_{\text{CM}}$	C promoting M	8			Fit initial rescue speed
$\hat{C}_R$	Threshold CDC-42 level for branched actin	0.25			Between A and P levels
$\hat{R}_{\text{CR}}$	CDC-42 producing branched actin rate	1			Arbitrary
$\hat{R}_{\text{RR}}$	Autocatalytic branched actin strength	5			Equal strength to nucleation
$\hat{R}_{\text{R}\sigma}$	Branched actin inhibiting myosin rate	10			Fit boundary position

Table 3: Additional parameters for coupled model (M17) with branched actin additions in (M18).

3.1 Incorporating branched actin

In the dimensionless form of (M17), the model we used for branched actin is

$$\partial_{\hat{t}}\hat{R}+\hat{\sigma}_0\partial_{\hat{x}}\left(\hat{v}\hat{R}\right) = \tag{M18a}$$
$$\hat{D}_R\partial_{\hat{x}}^2\hat{R} + \hat{R}_{\text{CR}}\max\left(\hat{C}-\hat{C}_R,0\right)\left(1+\hat{R}_{\text{RR}}\hat{R}\right)\left(1-\int_0^1 \hat{R}(x)\,dx\right) - \hat{K}_R^{\text{off}}\hat{R},$$

$$\hat{D}_R = \frac{D_R}{L^2 k_A^{\text{dp}}}, \quad R_{\text{CR}} = \frac{r_{\text{CR}}C^{(\text{Tot})}}{k_A^{\text{dp}}}, \quad R_{\text{RR}} = \frac{r_{\text{RR}}R^{(\text{Tot})}}{r_{\text{CR}}}, \quad \hat{K}_R^{\text{off}} = \frac{k_R^{\text{off}}}{k_A^{\text{dp}}}. \tag{M18b}$$

$$\hat{\sigma}_a = \frac{\hat{M}}{1+\hat{R}_{\text{R}\sigma}\hat{R}}. \tag{M18c}$$

We use division of the stress instead of subtraction because, as the branched actin concentration goes to infinity, we expect the tension to approach zero, as was shown to be the case *in vitro* using laser ablation [9].

To assign values to the unknown parameters, we assume that branched actin diffuses at the same level as CDC-42, and that the bound lifetime is about 8 s. This gives $D_R = 0.1\ \mu\text{m/s}^2$ and $k_R^{\text{off}} = 0.12$. We set the CDC-42 threshold for branched actin nucleation to be between anterior and posterior levels (see Fig. 3 main text), giving $\hat{C}_R = 0.25$. The base level of branched actin production is arbitrary; so we simply set $\hat{R}_{\text{CR}} = 1$, which gives a branched actin level around 0.2 on the anterior. We then assume that branched actin autocatalytic activity makes an equal contribution (relative to CDC-42 nucleation) to the overall branched actin, meaning $\hat{R}_{\text{RR}}\hat{R} = 1$. Since $\hat{R} \approx 0.2$, we get $\hat{R}_{\text{RR}} = 5$. Finally, we set $\hat{R}_{\text{R}\sigma} = 10$, so that the myosin boundary sits roughly at half the domain length. The simulation that results with these parameter values is shown in Fig. 6 of the main text.

References

[1] Justin S Bois, Frank Jülicher, and Stephan W Grill. Pattern formation in active fluids. *Biophysical Journal*, 100(3):445a, 2011.

[2] Nathan W Goehring, Philipp Khuc Trong, Justin S Bois, Debanjan Chowdhury, Ernesto M Nicola, Anthony A Hyman, and Stephan W Grill. Polarization of par proteins by advective triggering of a pattern-forming system. *Science*, 334(6059):1137–1141, 2011.

[3] Peter Gross, K Vijay Kumar, Nathan W Goehring, Justin S Bois, Carsten Hoege, Frank Jülicher, and Stephan W Grill. Guiding self-organized pattern formation in cell polarity establishment. *Nature physics*, 15(3):293–300, 2019.

[4] Rukshala Illukkumbura, Nisha Hirani, Joana Borrego-Pinto, Tom Bland, KangBo Ng, Lars Hubatsch, Jessica McQuade, Robert G Endres, and Nathan W Goehring. Design principles for selective polarization of par proteins by cortical flows. *Journal of Cell Biology*, 222(8), 2023.

[5] Charles F Lang, Alexander Anneken, and Edwin Munro. Oligomerization and feedback on membrane recruitment stabilize par-3 asymmetries in c. elegans zygotes. *bioRxiv*, pages 2023–08, 2023.

[6] Charles F Lang and Edwin Munro. The par proteins: from molecular circuits to dynamic self-stabilizing cell polarity. *Development*, 144(19):3405–3416, 2017.

[7] Charles F Lang and Edwin M Munro. Oligomerization of peripheral membrane proteins provides tunable control of cell surface polarity. *Biophysical Journal*, 121(23):4543–4559, 2022.

[8] Mirjam Mayer, Martin Depken, Justin S Bois, Frank Jülicher, and Stephan W Grill. Anisotropies in cortical tension reveal the physical basis of polarizing cortical flows. *Nature*, 467(7315):617–621, 2010.

[9] Camelia G Muresan, Zachary Gao Sun, Vikrant Yadav, A Pasha Tabatabai, Laura Lanier, June Hyung Kim, Taeyoon Kim, and Michael P Murrell. F-actin architecture determines constraints on myosin thick filament motion. *Nature communications*, 13(1):7008, 2022.

[10] François B Robin, William M McFadden, Baixue Yao, and Edwin M Munro. Single-molecule analysis of cell surface dynamics in caenorhabditis elegans embryos. *Nature methods*, 11(6):677–682, 2014.

[11] Arnab Saha, Masatoshi Nishikawa, Martin Behrndt, Carl-Philipp Heisenberg, Frank Jülicher, and Stephan W Grill. Determining physical properties of the cell cortex. *Biophysical journal*, 110(6):1421–1429, 2016.

[12] Anne Sailer, Alexander Anneken, Younan Li, Sam Lee, and Edwin Munro. Dynamic opposition of clustered proteins stabilizes cortical polarity in the c. elegans zygote. *Developmental cell*, 35(1):131–142, 2015.